JCIM JOURNAL OF CHEMICAL INFORMATION AND MODELING

Article

Cite This: J. Chem. Inf. Model. 2018, 58, 2477−2490

pubs.acs.org/jcim

# AFLOW-CHULL: Cloud-Oriented Platform for Autonomous Phase Stability Analysis

Corey Oses,[†] Eric Gossett,[†] David Hicks,[†] Frisco Rose,[†] Michael J. Mehl,[‡] Eric Perim,[†] Ichiro Takeuchi,[§,∥] Stefano Sanvito,[⊥] Matthias Scheffler,[#] Yoav Lederer,[†,▽] Ohad Levy,[†,▽] Cormac Toher,[†] and Stefano Curtarolo*[,†,#]

[†]Department of Mechanical Engineering and Materials Science and Center for Materials Genomics, Duke University, Durham, North Carolina 27708, United States

[‡]United States Naval Academy, Annapolis, Maryland 21402, United States

[§]Department of Materials Science and Engineering, University of Maryland, College Park, Maryland 20742-4111, United States

[∥]Center for Nanophysics and Advanced Materials, University of Maryland, College Park, Maryland 20742, United States

[⊥]School of Physics, AMBER and CRANN Institute, Trinity College, Dublin 2, Ireland

[#]Fritz-Haber-Institut der Max-Planck-Gesellschaft, 14195 Berlin-Dahlem, Germany

[▽]Department of Physics, NRCN, P.O. Box 9001, Beer-Sheva 84190, Israel

Supporting Information

**ABSTRACT:** A priori prediction of phase stability of materials is a challenging practice, requiring knowledge of all energetically competing structures at formation conditions. Large materials repositories—housing properties of both experimental and hypothetical compounds—offer a path to prediction through the construction of informatics-based, ab initio phase diagrams. However, limited access to relevant data and software infrastructure has rendered thermodynamic characterizations largely peripheral, despite their continued success in dictating synthesizability. Herein, a new module is presented for autonomous thermodynamic stability analysis, implemented within the open-source, ab initio framework AFLOW. Powered by the AFLUX Search-API, AFLOW-CHULL leverages data of more than 1.8 million compounds characterized in the AFLOW.org repository, and can be employed locally from any UNIX-like computer. The module integrates a range of functionality: the identification of stable phases and equivalent structures, phase coexistence, measures for robust stability, and determination of decomposition reactions. As a proof of concept, thermodynamic characterizations have been performed for more than 1300 binary and ternary systems, enabling the identification of several candidate phases for synthesis based on their relative stability criterion—including 17 promising $C15_b$-type structures and 2 half-Heuslers. In addition to a full report included herein, an interactive, online web application has been developed showcasing the results of the analysis and is located at aflow.org/aflow-chull.

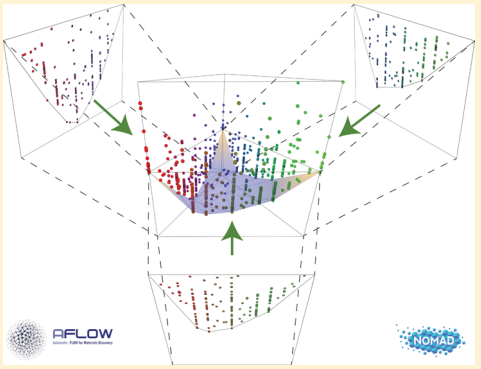


## 1. INTRODUCTION

Accelerating the discovery of new functional materials demands an efficient determination of synthesizability. Generally, materials synthesis is a multifaceted problem, spanning (i) technical challenges, such as experimental apparatus design and growth conditions,[1,2] as well as (ii) economic and environmental obstacles, including accessibility and handling of necessary components.[3,4] Phase stability is a limiting factor. Often, it accounts for the gap between materials prediction and experimental realization. Addressing stability requires an understanding of how phases compete thermodynamically. Despite the wealth of available experimental phase diagrams,[5] the number of systems explored represents a negligible fraction of all hypothetical structures.[6,7] Large materials databases[8−16] enable the construction of calculated phase diagrams, where aggregate structural and energetic materials data are employed. The analysis delivers many fundamental thermodynamic descriptors, including stable/unstable classification, phase coexistence, measures of robust stability, and determination of decomposition reactions.[4,17−20]

As with all informatics-based approaches, ab initio phase diagrams require an abundance of data: well-converged enthalpies from a variety of different phases. Many thermodynamic descriptors computed from the AFLOW.org repository have already demonstrated predictive power in characterizing

Special Issue: Materials Informatics

Received: June 18, 2018
Published: September 6, 2018






DOI: 10.1021/acs.jcim.8b00393
J. Chem. Inf. Model. 2018, 58, 2477−2490

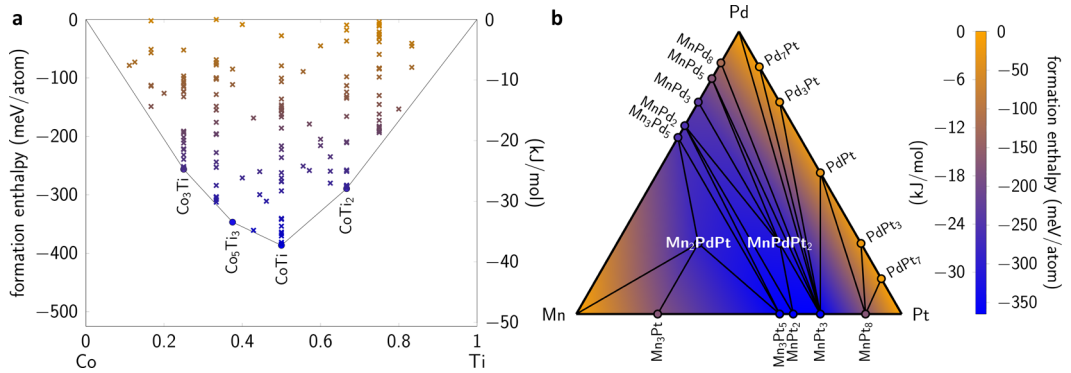


**Figure 1.** Example hull illustrations in two and three dimensions, generated by AFLOW-CHULL: (a) Co−Ti and (b) Mn−Pd−Pt.

phase stability,[4,17,21−34] including one investigation that resulted in the synthesis of two new magnets—the first ever discovered by computational approaches.[4] As exploration embraces more-complex systems, such analyses are expected to become increasingly critical in confining the search space. In fact, prospects for stable ordered phases diminish with every new component (dimension), despite the growing number of combinations. This is due to increased competition with (i) phases of lower dimensionality, e.g., ternary phases competing with stable binary phases,[34] and (ii) disordered (higher-entropy) phases.[35−37]

To address the challenge, a new module has been implemented in the autonomous, open-source[38] AFLOW (Automatic Flow) framework for ab initio calculations.[21,23−25,29,39−44] AFLOW-CHULL (AFLOW convex hull) offers a thermodynamic characterization that can be employed locally from any UNIX-like machine, including those running Linux and macOS. Built-in data curation and validation schemes ensure results that are well-converged: adhering to proper hull statistics, performing outlier detection, and determining structural equivalence. AFLOW-CHULL is powered by the AFLUX Search-API (application programming interface),[11] which enables access to more than 1.8 million compounds from the AFLOW.org repository. With AFLUX integration, data bindings are flexible enough to serve any materials database, including large heterogeneous repositories such as NOMAD.[12]

Several analysis output types have been created for integration into a variety of design workflows, including plain text and JSON (JavaScript Object Notation) file types. A small set of example scripts have been included demonstrating how to employ AFLOW-CHULL from within a Python environment, much in the spirit of AFLOW-SYM.[45] The JSON output also powers an interactive, online web application offering enhanced presentation of thermodynamic descriptors and visualization of two- and three-dimensional hulls. The application can be accessed through the AFLOW.org portal under "Apps and Docs" or directly at aflow.org/aflow-chull.

As a test-bed, the module is applied to all 1.8 million compounds available in the AFLOW.org repository. After enforcing stringent hull convergence criteria, the module resolves a thermodynamic characterization for more than 1300 binary and ternary systems. Stable phases are screened for previously explored systems and ranked by their relative stability criterion, a dimensionless quantity capturing the effect of the phase on the minimum energy surface.[4] Several promising candidates are identified, including 17 $C15_b$-type structures ($F\bar{4}3m$, No. 216) and 2 half-Heuslers. Hence, screening criteria based on these thermodynamic descriptors can accelerate the discovery of new stable phases. More broadly, the design of more challenging materials, including ceramics[46] and metallic glasses,[31] benefit from autonomous, integrated platforms such as AFLOW-CHULL.

## 2. METHODS

**2.1. Defining Thermodynamic Stability.** For a multi-component system at a fixed temperature ($T$) and pressure ($p$), the minimum Gibbs free energy $G$ (per atom) defines the thermodynamic equilibrium:

$$G(T, p, \{x_i\}) = H - TS \tag{1}$$

where $x_i$ is the atomic concentration of species $i$, $H$ the enthalpy, and $S$ the entropy. A binary phase $A_{x_A}B_{x_B}$ is stable at equilibrium with respect to its components $A$ and $B$ if the corresponding formation reaction releases energy:

$$x_A A + x_B B \xrightarrow{\Delta G < 0} A_{x_A}B_{x_B} \tag{2}$$

where $\Delta G$ is the energy difference between the mixed phase and the sum of its components. Conversely, a positive $\Delta G$ suggests that the decomposition of $A_{x_A}B_{x_B}$ is preferred and, therefore, is unstable. Generally, the magnitude of $\Delta G$ quantifies the propensity for the reaction, and the sign determines the direction.

Relative stability can be visualized on a free-energy-concentration diagram—$G$ vs $\{x_i\}$—where $\Delta G$ is depicted as the energetic vertical-distance between $A_{x_A}B_{x_B}$ and the tie-line connecting end-members (elemental phases) $A$ and $B$. End-members constitute only a single pathway to formation/decomposition, and all feasible reactions should be considered for system-wide stability. Identification of equilibrium phases is mathematically equivalent to the construction of the convex hull—the set of the most extreme or "outside" points (see Figure 1a). The convex hull characterizes the phase stability of the system at equilibrium and does not include kinetic considerations for synthesis. Growth conditions affect the final outcome leading to formation of polymorphs and/or metastable phases, which could differ from the equilibrium phases. This is a formidable task for high-throughput characterization. To help identify kinetic pathways for synthesis, AFLOW-CHULL includes (more in future releases) potential kinetic descriptors, e.g., chemical decompositions, distance from stability, entropic temperature,[48] glass formation ability,[31] and spectral entropy analysis for high-entropy systems.

In the zero temperature limit (as is the case for ground-state density functional theory), the entropic term of eq 1 vanishes,


DOI: 10.1021/acs.jcim.8b00393
J. Chem. Inf. Model. 2018, 58, 2477−2490

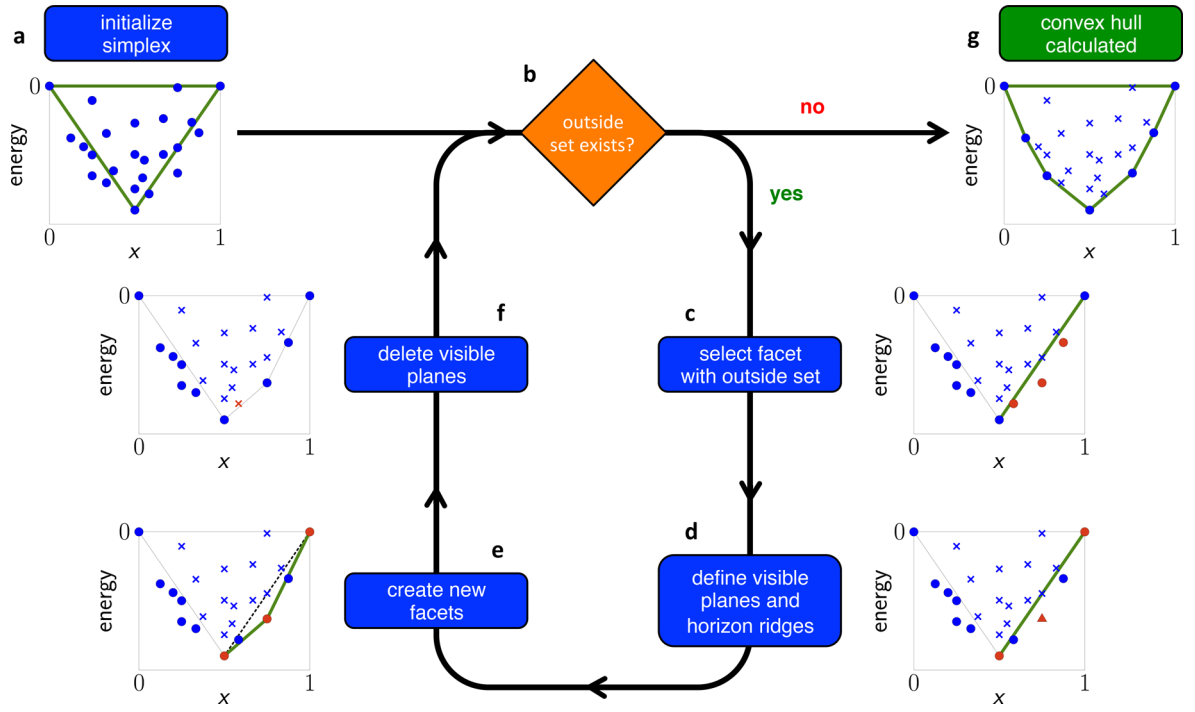


**Figure 2.** Illustration of the convex hull construction for a binary system with AFLOW-CHULL. The approach is inspired by the Qhull algorithm.[47] The points on the plot represent structures from the AFLOW.org database.[8−11] Steps (a) and (g) denote the beginning and end of the algorithm, respectively. Steps (c−f) denote the iterative loop that continues until the condition denoted by step (b) is no longer satisfied. Points are marked with crosses if, by that step in the algorithm, they have been determined to be inside the hull; otherwise, they are marked with circles. The furthest point from the facet in step (d) is marked with a triangle. Points and facets of interest are highlighted in red and green, respectively.

leaving the formation enthalpy term (per atom) as the driving force:

$$H_f = H_{A_{x_A}B_{x_B}} - (x_A H_A + x_B H_B) \tag{3}$$

By construction, formation enthalpies of stable elemental phases are zero, restricting the convex hull to the lower hemisphere. Zero-point energies are not yet included in the AFLOW.org repository and, therefore, are neglected from the enthalpy calculations. Efforts to incorporate vibrational characterizations are underway.[49,50] This contribution could have a large impact on compounds containing light elements, such as hydrogen,[51] which comprise a small minority (<1%) of the overall repository.

By offsetting the enthalpy with that of the elemental phases, $H_f$ quantifies the energy gain from forming new bonds between unlike components,[52] e.g., $A-B$. Currently, the AFLOW-CHULL framework does not allow the renormalization of chemical potentials to improve the calculation of formation enthalpies when gas phases are involved. A new first-principles approach is being developed and tested in AFLOW, and will be implemented in future versions of the AFLOW-CHULL software, together with the available approaches.[53,54]

The tie-lines connecting stable phases in Figure 1a define regions of phase separation where the two phases coexist at equilibrium. The chemical potentials are equal for each component among coexisting phases, implying the common tangent tie-line construction.[55,56] Under thermodynamic equilibrium, phases above a tie-line will decompose into a linear combination of the stable phases that define the tie-line (see Figure 4d, presented later in this work). The Gibbs phase rule[57] dictates the shape of tie-lines for $N$-ary systems, which generalizes to $(N-1)$-dimensional triangles (simplexes) and correspond to facets of the convex hull, e.g., lines in two dimensions (Figure 1a), triangles in three dimensions (Figure 1b), and tetrahedra in four dimensions. The set of equilibrium facets define the $N$-dimensional minimum energy surface.

**2.2. Hull Construction.** AFLOW-CHULL calculates the $N$-dimensional convex hull corresponding to an $N$-ary system with an algorithm partially inspired by Qhull.[47] The algorithm is efficient in identifying the most important points for construction of facets, which are treated as hyperplanes instead of boundary-defining inequalities. AFLOW-CHULL uniquely accommodates thermodynamic hulls, i.e., data occupying the lower half hemisphere and defined by stoichiometric coordinates ($0 \leq x_i \leq 1$). Points corresponding to individual phases are characterized by their stoichiometric and energetic coordinates:

$$\mathbf{p} = [x_1, x_2, ..., x_{N-1}, H_f] = [\mathbf{x}, H_f] \tag{4}$$

where $x_N$ is implicit ($\sum_i x_i = 1$). Data preparation includes (i) the elimination of phases that are unstable with respect to end-members (points above the zero $H_f$ tie-line), and (ii) organization of phases by stoichiometry and sorted by energy. Through this stoichiometry group structure, all but the minimum energy phases are eliminated from the convex hull calculation.

The workflow is illustrated in Figure 2. AFLOW-CHULL operates by partitioning space, iteratively defining "inside" versus "outside" half-spaces until all points are either on the hull or inside of it. First, a simplex is initialized (Figure 2, step (a)) with the most extreme points: stable end-members and the globally stable mixed phase (lowest energy). A facet is described as

$$\mathbf{n}\cdot\mathbf{r} + D = 0 \tag{5}$$

where $\mathbf{n}$ is the characteristic normal vector, $\mathbf{r}$ is the position vector, and $D$ is the offset. A general hyperplane is defined by $N$ points and $k = (N-1)$ corresponding edges $\mathbf{v}_k = \mathbf{p}_k - \mathbf{p}_{origin}$. To



DOI: 10.1021/acs.jcim.8b00393
J. Chem. Inf. Model. 2018, 58, 2477−2490

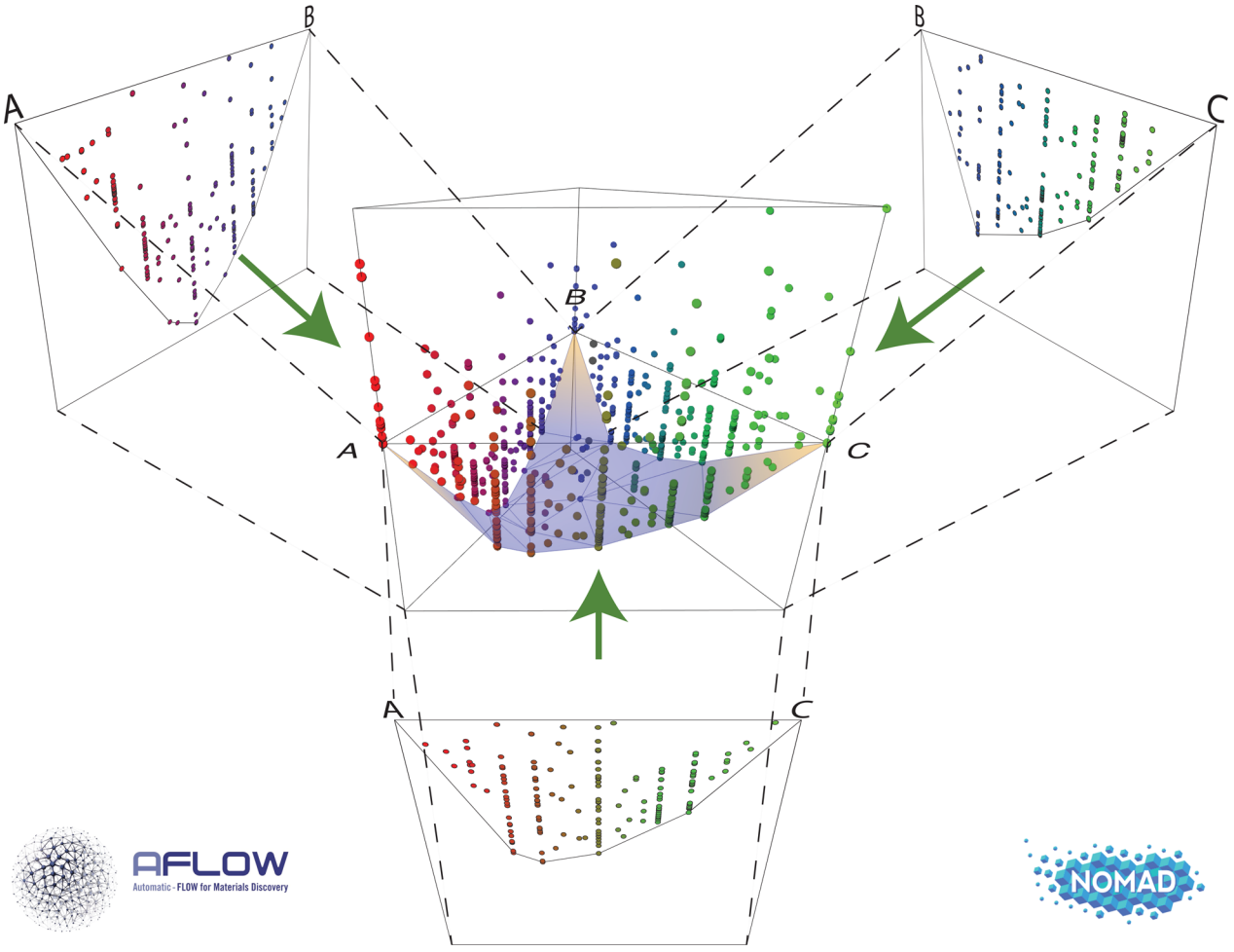


**Figure 3.** Illustration of the AFLOW-CHULL iterative hull scheme. The convex hull and associated properties are first calculated for the binary hulls, and then propagated to the ternary hull. This is generalized for $N$ dimensions.

construct $\mathbf{n}$, AFLOW-CHULL employs a generalized cross-product approach,[58] where $n_{i\in\{1,\ldots,N\}}$ (unnormalized) is the $i$-row cofactor of the matrix $\mathbf{V}$ containing $\mathbf{v}_k$ in its columns:

$$n_i = (-1)^{i+1} M_{i,j=0}\left(\begin{bmatrix} | & & | \\ \mathbf{v}_1 & \cdots & \mathbf{v}_k \\ | & & | \end{bmatrix}\right) \tag{6}$$

Here, $M_{i,j=0}(\mathbf{V})$ denotes the $i$-row minor of $\mathbf{V}$, i.e., the determinant of the submatrix formed by removing row $i$.

The algorithm then enters a loop over the facets of the convex hull until no points are declared "outside", defined in the hyperplane description by the signed point-plane distance (see Figure 2, step (b)). Each point outside of the hull is singularly assigned to the outside set of a facet (shown in red in Figure 2, step (c)). The furthest point from each facet—by standard point-plane distance—is selected from the outside set (marked with a triangle in Figure 2, step (d)). Each neighboring facet is visited to determine whether the furthest point is also outside of it, defining the set of visible planes (shown in green in Figure 2) and its boundary, the horizon ridges (shown in red in Figure 2, step (d)). The furthest point is combined with each ridge of the horizon to form new facets (Figure 2, step (e)). The visible planes—the dotted line in Figure 2, step (e)—are then removed from the convex hull (Figure 2, step (f)). The fully constructed convex hull—with all points on the hull or inside of it—is summarized in Figure 2, step (g).

A challenge arises with lower dimensional data in higher dimensional convex hull constructions. For example, binary phases composed of the same species all exist on the same (vertical) plane in three dimensions. A half-space partitioning scheme can make no "inside" versus "outside" differentiation between such points. These ambiguously defined facets[59] constitute a hull outside the scope of the Qhull algorithm.[47] In the case of three dimensions, the creation of ill-defined facets with collinear edges can result. Hyper-collinearity—planes defined with collinear edges, tetrahedra defined with coplanar faces, etc.—is prescribed by the content (hyper-volume) of the facet. The quantity resolves the length of the line (1-simplex), the area of a triangle (2-simplex), the volume of a tetrahedron (3-simplex), etc., and is calculated for a simplex of $N$-dimensions via the Cayley−Menger determinant.[60] Both vertical and content-less facets are problematic for thermodynamic characterizations, particularly when calculating hull distances, which require facets within finite energetic distances and well-defined normals.

A dimensionally iterative scheme is implemented in AFLOW-CHULL to solve the issue. It calculates the convex hull for each dimension consecutively (Figure 3). In the case of a ternary hull, the three binary hulls are calculated first, and the relevant thermodynamic data is extracted and then propagated forward. Although vertical and content-less facets are still created in higher



DOI: 10.1021/acs.jcim.8b00393
J. Chem. Inf. Model. 2018, 58, 2477−2490

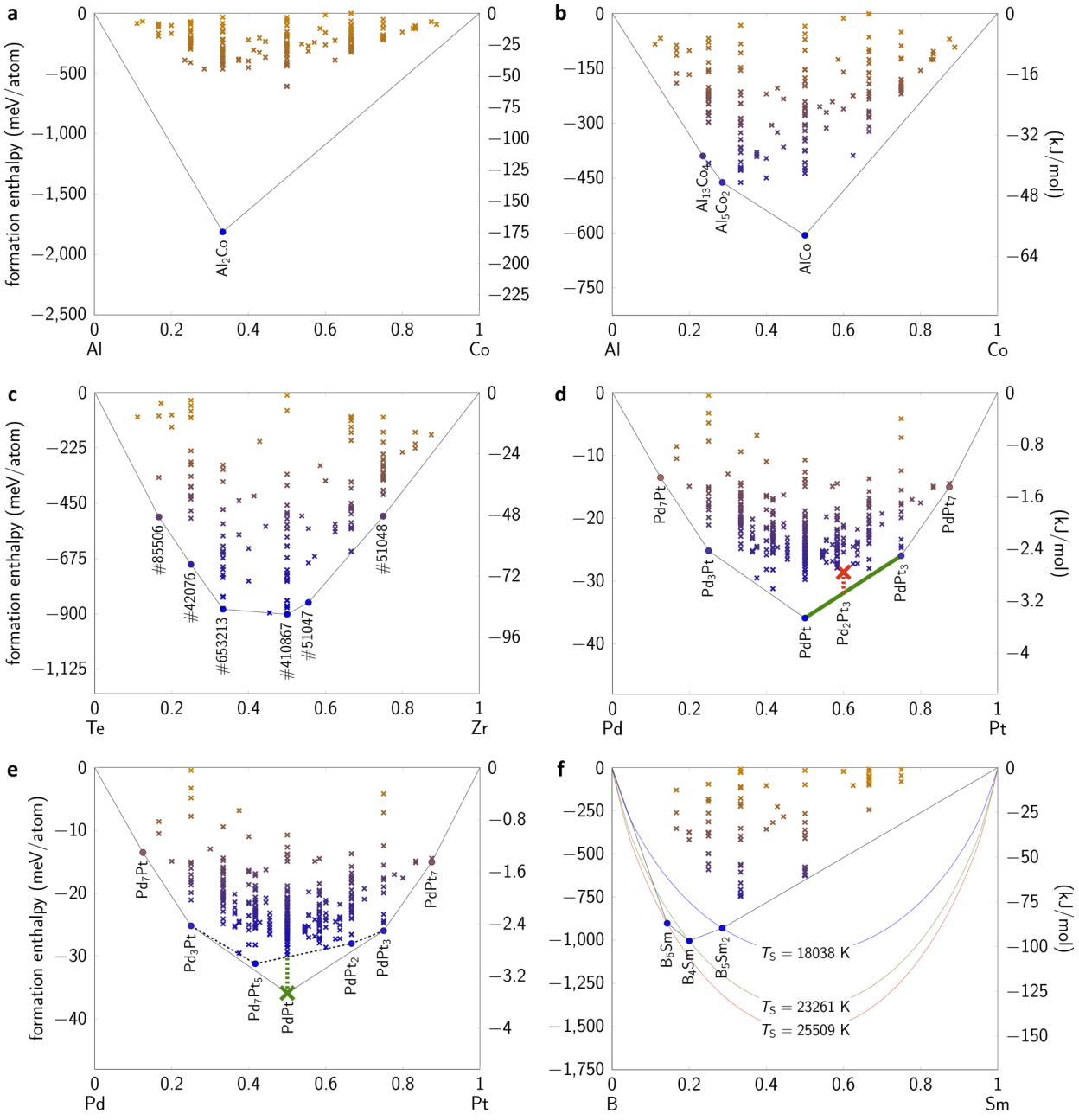


**Figure 4.** Illustrations of various automated convex hull analyses in AFLOW-CHULL: (a) plot showing an egregious outlier in the Al−Co convex hull; (b) corrected Al−Co convex hull with the outlier removed; and (c) Te−Zr convex hull with the traditional compound labels replaced with the corresponding ICSD number designations, as determined by a structure comparison analysis (if multiple ICSD entries are found for the same stoichiometry, the lowest number ICSD entry is chosen (usually reported chronologically)). Panels (d−e) show the Pd−Pt convex hull. (d) The decomposition energy of $Pd_2Pt_3$ is plotted in red, and the equilibrium facet directly below it is highlighted in green. The facet is defined by ground-state phases $PdPt_3$ and PdPt. (e) The stability criterion $\delta_{sc}$ of PdPt is plotted in green, with the pseudohull plotted with dashed lines. In panel (f), the B−Sm convex hull is plotted with the ideal "*iso-max-latent-heat*" lines of the grand canonical ensemble[29,48] for the ground-state structures.

dimensions, no thermodynamic descriptors are extracted from them. To optimize the calculation, only stable binary structures are propagated forward to the ternary hull calculation, and this approach is generalized for $N$ dimensions. The scheme is the default for thermodynamic hulls, resorting back to the general convex hull algorithm otherwise.

**2.3. Thermodynamic Data.** Structural and energetic data employed to construct the convex hull is retrieved from the AFLOW.org[8−11] repository, which contains more than 1.8 million compounds and 180 million calculated properties. The database is generated by the autonomous, ab initio AFLOW framework[21,23−25,29,39−44] following the AFLOW Standard for high-throughput materials science calculations.[10] In particular, calculations are performed with VASP (Vienna Ab initio Simulation Package).[61] Wave functions are represented by a large basis set, including all terms with kinetic energy up to a threshold 1.4 times larger than the recommended defaults. AFLOW also leverages a large **k**-point mesh—as standardized by a **k**-points-per-reciprocal-atom scheme[10]—which is critical for convergence and reliability of calculated properties. Investigations show that the AFLOW Standard of at least 6000 **k**-points per reciprocal atom for structural relaxations and 10 000 for the



DOI: 10.1021/acs.jcim.8b00393
J. Chem. Inf. Model. 2018, 58, 2477−2490

static calculations ensures robust convergence of the energies to within 1 meV/atom in more than 95% of systems (including metals which suffer from the discontinuity in the occupancy function at zero temperature), and within 3 meV/atom otherwise.[62]

Special consideration is taken for the calculation of $H_f$. The reference energies for the elemental phases are calculated and stored in the LIB1 catalog for unary phases in the AFLOW.org repository, and include variations for different functionals and pseudopotentials. For consistency, AFLOW-CHULL only employs data calculated with the Perdew−Burke−Ernzerhof Generalized Gradient Approximation functional[63] and pseudopotentials calculated with the projector augmented wave method[64] (PAW-PBE). Calculations employing DFT+$U$ corrections to rectify self-interaction errors and energy-gap issues for electronic properties[10] are neglected. Generally, these corrections are parametrized and material-specific.[65] They artificially augment the energy of the system affecting the reliability of thermodynamic properties. It is possible to encounter stable (lowest energy) elemental phases with energy differences from the reference of order meV/atom, which is the result of duplicate entries (by relaxation or otherwise) as well as reruns with new parameters, e.g., a denser **k**-point mesh. To avoid any issues with the convex hull calculation, the algorithm fixes the half-space plane at zero. However, a "warning" is prompted in the event that the stable elemental phase differs from the reference energy by more than 15 meV/atom, yielding a "skewed" hull.

Data are retrieved via the AFLUX Search-API,[11] designed for accessing property-specific datasets efficiently. The following is an example of a relevant request: http://aflowlib.duke.edu/search/API/?species(Mn,Pd),nspecies(2),*,paging(0), where http://aflowlib.duke.edu/search/API/ is the URL for the AFLUX server and "species(Mn,Pd),nspecies(2),*,paging(0)" is the query. Species(Mn,Pd) queries for any entry containing the elements Mn or Pd, nspecies(2) limits the search to binaries only, * returns the data for all available fields, and paging(0) amalgamates all data into a single response without paginating (warning, this can be a large quantity of data). Such queries are constructed combinatorially for each dimension, e.g., a general ternary hull $ABC$ constructs the following seven queries: species($A$), species($B$), and species($C$) with nspecies(1), species($A$,$B$), species($A$,$C$), and species($B$,$C$) with nspecies(2), and species($A$,$B$,$C$) with nspecies(3).

**2.4. Validation Schemes.** Various statistical analyses and data curation procedures are employed by AFLOW-CHULL to maximize fidelity. At a minimum, each binary hull must contain 200 structures to ensure a sufficient sampling size for inference. There is never any guarantee that all stable structures have been identified,[29,66] but convergence is approached with larger datasets. With continued growth of LIB3 (ternary phases) and beyond, higher dimensional parameters will be incorporated, although it is expected that the parameters are best-defined along tie-lines (versus tie-surfaces). A comprehensive list of available alloys and structure counts are included in the Supporting Information.

**2.5. Outlier Detection.** In addition to having been calculated with a standard set of parameters,[10] database entries should also be well-converged. Prior to the injection of new entries into the AFLOW.org database, various verification tests are employed to ensure convergence, including an analysis of the relaxed structure's stress tensor.[11] Issues stemming from poor convergence and failures in the functional parametrization[17,66] can change the topology of the convex hull, resulting in contradictions with experiments. Hence, an outlier detection algorithm is applied before the hull is constructed: structures are classified as outliers and discarded if they have energies that fall well below the first quartile by a multiple of the interquartile range (conservatively set to 3.25 by default).[67] Only points existing in the lower half-space (phases stable against end-members) are considered for the outlier analysis, and hence systems need to show some miscibility, i.e., at least four points for a proper interquartile range determination. Despite its simplicity, the interquartile range is the preferred estimate of scale over other measures such as the standard deviation or the median absolute deviation, which require knowledge of the underlying distribution (normal or otherwise).[68] An example hull (Al−Co) showing an outlier is plotted in Figure 4a, and the corrected hull with the outlier removed is presented in Figure 4b.

**2.6. Duplicate Detection.** A procedure for identifying duplicate entries is also employed. By database construction, near-exact duplicates of elemental phases exist in LIB2, which is created by spanning the full range of compositions for each alloy system (including elemental phases). These degenerate entries are detected and removed by comparing composition, prototype, and formation enthalpy. Other structures may have been created distinctly, but converge to duplicates via structural relaxation. These equivalent structures are detected via AFLOW-XTALMATCH (AFLOW crystal match),[69] which determines structural/material uniqueness via the Burzlaff criteria.[70] To compare two crystals, a commensurate representation between structures is resolved by (i) identifying common unit cells, (ii) exploring cell orientations and origin choices, and (iii) matching atomic positions. For each description, the structural similarity is measured by a composite misfit quantity based on the lattice deviations and mismatch of the mapped atomic positions, with a match occurring for sufficiently small misfit values (<0.1). Depending on the size of the structures, the procedure can be quite expensive, and only applied to find duplicate stable structures. Candidates are first screened by composition, space group, and formation enthalpies (must be within 15 meV/atom of the relevant stable configuration). By identifying duplicate stable phases, AFLOW-CHULL can cross-reference the AFLOW.org ICSD (Inorganic Crystal Structure Database) catalog[71,72] to reveal whether the structure has already been observed. The analysis is depicted in Figure 4c, where the Te−Zr convex hull is plotted with the compound labels replaced by the corresponding ICSD number designation.

**2.7. Thermodynamic Descriptors.** A wealth of properties can be extracted from the convex hull construction beyond a simple determination of stable/unstable phases. For unstable structures, the energetic vertical distance to the hull $\Delta H_f$, depicted in Figure 4d, serves as a useful metric for quasi-stability. $\Delta H_f$ is the magnitude of the energy driving the decomposition reaction. Without the temperature and pressure contributions to the energy, near-stable structures should also be considered (meta-)stable candidates, e.g., those within $k_BT = 25$ meV (room temperature) of the hull. Highly disordered systems can be realized with even larger distances.[17,73]

To calculate $\Delta H_f$ of phase $\mathbf{p}$ (eq 4), AFLOW-CHULL first resolves the energy of the hull $H_{hull}$ at stoichiometric coordinates $\mathbf{x}$, and then subtracts it from the phase's formation enthalpy $H_f$:

$$\Delta H_f[\mathbf{p}] = |H_f - H_{hull}[\mathbf{x}]| \tag{7}$$

The procedure is depicted in Figure 4d, which involves identifying the facet (highlighted in green) that encloses $\mathbf{x}$ and thus defines $H_{hull}(\mathbf{x})$. Here, the hyperplane description can be


DOI: 10.1021/acs.jcim.8b00393
J. Chem. Inf. Model. 2018, 58, 2477−2490

| prototype | auid | original space group | relaxed space group | spin ($\mu_B$/atom) | $H_f$ (meV/atom) | $T_S$ (K) | $\Delta H_f$ (meV/atom) |
|---|---|---|---|---|---|---|---|
| ternaries | | | | | | | |
| $Ag_4AuCd$ | | | | | | | |
| T0010.ABC | aflow:f01a0242937da2ae | $F\bar{4}3m\#216$ | $F\bar{4}3m\#216$ | 0.00 | 87 | -1170 | 162 |
| decomposition reaction: | | | | $Ag_{0.6667}Au_{0.1667}Cd_{0.1667} \rightarrow 0.3333\ Ag + 0.6667\ Ag_{0.5}Au_{0.25}Cd_{0.25}$ | | | |
| $Ag_2AuCd$ (ground state) | | | | | | | $\delta_{sc} = 1$ meV/atom |
| TFCC016.ABC | aflow:b306fb2e8866a640 | $P4/mmm\#123$ | $P4/mmm\#123$ | 0.00 | -112 | 1251 | 0 |
| TFCC013.ABC | aflow:2f98e1c035b5aaaa | $I4/mmm\#139$ | $I4/mmm\#139$ | 0.00 | -111 | 1243 | 1 |
| TFCC008.ABC | aflow:5de326cf35c34568 | $I\bar{4}m2\#119$ | $I\bar{4}m2\#119$ | 0.00 | -111 | 1234 | 1 |
| TBCC016.ABC | aflow:8634edc55da7d9b0 | $P4/mmm\#123$ | $P4/mmm\#123$ | 0.00 | -111 | 1234 | 1 |
| TFCC005.ABC | aflow:132a4b97141e5820 | $Pmm2\#25$ | $Pmm2\#25$ | 0.00 | -92 | 1027 | 20 |
| TFCC011.ABC | aflow:76257f541c620495 | $C2/m\#12$ | $C2/m\#12$ | 0.00 | -92 | 1024 | 20 |
| T0002.A2BC | aflow:331ee0a425d1f5af | $F\bar{4}3m\#216$ | $F\bar{4}3m\#216$ | 0.00 | -88 | 982 | 24 |
| TFCC010.ABC | aflow:53b2d83b7d6af7ed | $Pmmm\#47$ | $Pmmm\#47$ | 0.00 | -84 | 937 | 28 |
| TFCC006.ABC | aflow:2b3a7e04149b217c | $Cm\#8$ | $Cm\#8$ | 0.00 | -83 | 930 | 29 |
| TFCC015.ABC | aflow:a0fe092060da4a0d | $Cmmm\#65$ | $Cmmm\#65$ | 0.00 | -78 | 874 | 34 |
| T0001.A2BC | aflow:8f5a6e202c08fce7 | $Fm\bar{3}m\#225$ | $Fm\bar{3}m\#225$ | 0.00 | -74 | 829 | 38 |
| TFCC007.ABC | aflow:62b2209e478e18d5 | $P4mm\#99$ | $P4mm\#99$ | 0.00 | -70 | 780 | 42 |
| TBCC006.ABC | aflow:45de8e0b667b4376 | $P4mm\#99$ | $P4mm\#99$ | 0.00 | -67 | 746 | 45 |
| TBCC011.ABC | aflow:9a39572049203457 | $P4/mmm\#123$ | $P4/mmm\#123$ | 0.00 | -59 | 655 | 53 |
| TFCC012.ABC | aflow:4ee48aff3119af41 | $P4/mmm\#123$ | $P4/mmm\#123$ | 0.00 | -58 | 644 | 54 |
| 3-phase equilibria: | | | | $Ag–Ag_4Cd–Ag_2AuCd$, $Ag–Ag_3Au–Ag_2AuCd$, $Ag_4Cd–Ag_3Cd–Ag_2AuCd$, $Ag_3Au–AgAu–Ag_2AuCd$, $Ag_3Cd–Ag_2AuCd–Au_2Cd_3$, $AgAu–Ag_2AuCd–AgAu_2Cd$, $Ag_2AuCd–AgAu_2Cd–AuCd$, and $Ag_2AuCd–AuCd–Au_2Cd_3$ | | | |

**Figure 5.** Excerpt from the Ag−Au−Cd thermodynamic analysis report. The document is generated by AFLOW-CHULL and showcases entry-specific data from the AFLOW.org database, as well as calculated thermodynamic descriptors. Structures highlighted in green are structurally equivalent stable structures, and those in orange are structurally similar (same relaxed space group). The working document includes a variety of links, including hyperlinks to the entry page of each phase (see prototypes) and links to relevant parts of the report (see decomposition reaction and $N$-phase equilibria).

misleading (see eqs 5 and 6) because it lacks information about facet boundaries. The enclosing facet is identified as that which minimizes the distance to the zero $H_f$ tie-line at $\mathbf{x}$:

$$H_{\text{hull}}[\mathbf{x}] = -\min_{\text{facets}\in\text{hull}} \left| n_N^{-1}\left(D + \sum_{i=1}^{N-1} n_i x_i\right)\right| \tag{8}$$

Vertical facets and those showing hyper-collinearity (having no content) are excluded from the calculation.

With the appropriate facet identified, the $l$ coefficients of the balanced decomposition reaction are derived to yield the full equation. The decomposition of an $N$-ary phase into $l-1$ stable phases defines an $(l \times N)$-dimensional chemical composition matrix $\mathbf{C}$, where $C_{j,i}$ is the atomic concentration of the $i$-species of the $j$-phase (the first of which is the unstable mixed phase). Take, for example, the decomposition of $Pd_2Pt_3$ to PdPt and $PdPt_3$ as presented in Figure 4d:

$$N_1 Pd_{0.4}Pt_{0.6} \rightarrow N_2 Pd_{0.5}Pt_{0.5} + N_3 Pd_{0.25}Pt_{0.75} \tag{9}$$

where $N_j$ is the balanced chemical coefficient for phase $j$. In this case, matrix $\mathbf{C}$ is defined as

$$\begin{bmatrix} x_{Pd} \in Pd_2Pt_3 & x_{Pt} \in Pd_2Pt_3 \\ -x_{Pd} \in PdPt & -x_{Pt} \in PdPt \\ -x_{Pd} \in PdPt_3 & -x_{Pt} \in PdPt_3 \end{bmatrix} = \begin{bmatrix} 0.4 & 0.6 \\ -0.5 & -0.5 \\ -0.25 & -0.75 \end{bmatrix} \tag{10}$$

where a negative sign differentiates the right-hand side of the equation from the left. Reference 74 shows that $N_j$ can be extracted from the null space of $\mathbf{C}$. AFLOW-CHULL accesses the null space via a full $\mathbf{QR}$ decomposition of $\mathbf{C}$, specifically employing a general Householder algorithm.[75] The last column of the $(l \times l)$-dimensional $\mathbf{Q}$ orthogonal matrix spans the null space $\mathbf{N}$:

$$\mathbf{Q} = \begin{bmatrix} | & | & 0.8111 \\ \mathbf{q}_1 & \mathbf{q}_2 & 0.4867 \\ | & | & 0.3244 \end{bmatrix} \tag{11}$$

By normalizing $\mathbf{N}$ such that the first element $N_1 = 1$, the approach yields $N_2 = 0.6$ and $N_3 = 0.4$, which indeed balances eq 9. These coefficients can be used to verify the decomposition energy observed in Figure 4d. The formation enthalpies of $Pd_2Pt_3$, PdPt, and $PdPt_3$ are −286 meV/(10 atoms), −72 meV/(2 atoms), and −104 meV/(4 atoms), respectively. The decomposition energy is calculated as

$$0.6H_f[PdPt] + 0.4H_f[PdPt_3] - H_f[Pd_2Pt_3] = -3\ \text{meV/atom} \tag{12}$$

For a given stable structure, AFLOW-CHULL determines the phases with which it is in equilibrium. For instance, PdPt is in two-phase equilibria with $Pd_3Pt$, as well as with $PdPt_3$ (Figure 4d). Phase coexistence plays a key role in defining a descriptor for precipitate-hardened superalloys. Candidates are chosen if a relevant composition is in two-phase equilibrium with the host matrix, suggesting that the formation of coherent precipitates in the matrix is feasible.[17,76]

An analysis similar to that quantifying instability ($\Delta H_f$) determines the robustness of stable structures. The stability criterion $\delta_{sc}$ is defined as the distance of a stable structure to the pseudohull constructed without it (Figure 4e). Its calculation is identical to that of $\Delta H_f$ for the pseudohull (eqs 7 and 8). This descriptor quantifies the effect of the structure on the minimum energy surface, as well as the structure's susceptibility to destabilization by a new phase that has yet to be explored. As with the decomposition analysis, $\delta_{sc}$ also serves to anticipate the effects of temperature and pressure on the minimum energy surface. The descriptor played a pivotal role in screening Heusler structures for new magnetic systems.[4] $\delta_{sc}$ calls for the recalculation of facets local to the structure and all relevant


DOI: 10.1021/acs.jcim.8b00393
J. Chem. Inf. Model. 2018, 58, 2477−2490

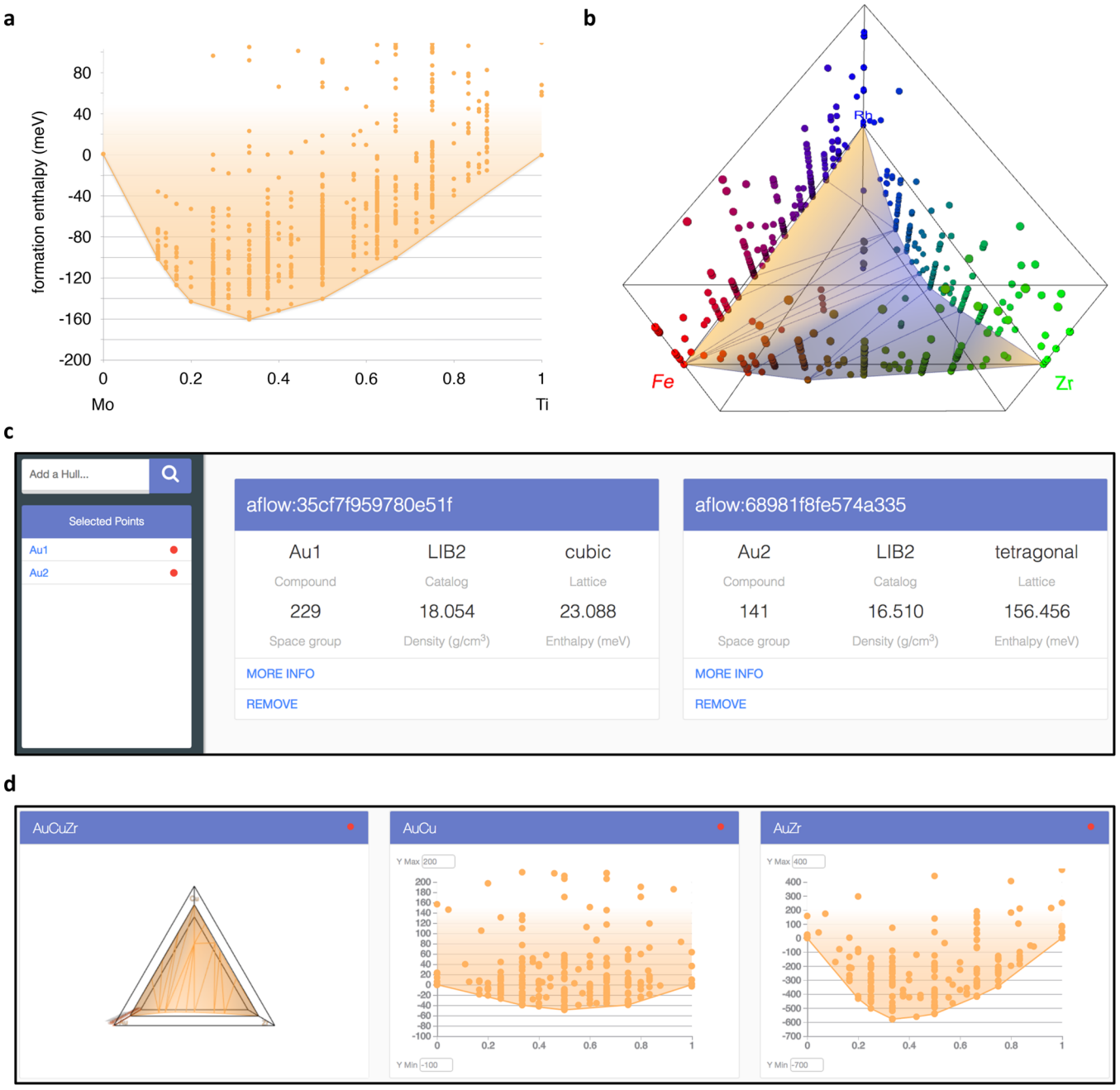


**Figure 6.** The convex hull web application powered by AFLOW-CHULL: (a) an example two-dimensional convex hull illustration (Mo−Ti); (b) an example three-dimensional convex hull illustration (Fe−Rh−Zr); (c) The information component of the hull application. Pertinent thermodynamic data for selected points is displayed within the grid of cards. Each card includes a link to the AFLOW.org entry page and the option to remove a point. As points are selected within the visualization, more cards will be added to the grid. (d) The comparison component of the hull application (each hull visualization is displayed as part of a grid of cards; from this page, new hulls can be added to the store by typing a query in the search box (sidebar)).

duplicates as well, thus employing the results of the structure comparison protocol.

AFLOW-CHULL can also plot the entropic temperature envelopes characterizing nucleation in hyperthermal synthesis methods for binary systems.[48] The entropic temperature is the ratio of the formation enthalpy to the mixing entropy for an ideal solution—a simple quantification for the resilience against disorder.[29] The ideal "*iso-max-latent-heat*" lines shown in Figure 4f try to reproduce the phase's capability to absorb latent heat, which can promote its nucleation over more-stable phases when starting from large Q reservoirs/feedstock. The descriptor successfully predicts the synthesis of $SmB_6$ over $SmB_4$ with hyperthermal plasma co-sputtering.[29,48]

## 3. RESULTS

**3.1. Analysis Output.** Following the calculation of the convex hull and relevant thermodynamic descriptors, AFLOW-CHULL generates a PDF file summarizing the results. Included in the PDF are (i) an illustration of the convex hull, as shown in Figure 1 (for binary and ternary systems),[77] and (ii) a report with the aforementioned calculated thermodynamic descriptors—an excerpt is shown in Figure 5.



DOI: 10.1021/acs.jcim.8b00393
J. Chem. Inf. Model. 2018, 58, 2477−2490

**Table 1. Listing of the 25 Binary Phases Predicted to Be Most Stable by AFLOW-CHULL[a]**

| compound[b] | auid | relaxed space group | $\lvert\delta_{sc}/H_f\rvert$ | comparison with ASM Alloy Phase Diagrams[5] |
|---|---|---|---|---|
| $Hf_5Pb$† | aflow:38ecc639e4504b9d | $P4/mmm$, No. 123 | 78% | no diagram |
| $AgIn_3$ | aflow:11ba11a3ee157f2e | $P6_3/mmc$, No. 194 | 54% | composition not found, nearest are $AgIn_2$ (space group $I4/mcm$, $\Delta H_f$ = 53 meV/atom) and In (space group $I4/mmm$) |
| $Hf_3In_4$† | aflow:1da75eb5f31b6dd5 | $P4/mbm$, No. 127 | 45% | no diagram |
| $AsTc_2$† | aflow:66dda41a34fe3ad6 | $C2/m$, No. 12 | 41% | no diagram |
| $MoPd_8$ | aflow:57e1a1246f813f27 | $I4/mmm$, No. 139 | 40% | composition not found, nearest are $Mo_{0.257}Pd_{0.743}$ (space group $Fm\bar{3}m$, POCC structure) and Pd (space group $Fm\bar{3}m$) |
| $Ga_4Tc$† | aflow:32051219452f8e0f | $Im\bar{3}m$, No. 229 | 39% | no diagram |
| $Pd_8V$ | aflow:7bd140d7b4c65bc1 | $I4/mmm$, No. 139 | 36% | composition not found, nearest are $V_{0.1}Pd_{0.9}$ (space group $Fm\bar{3}m$, POCC structure) and $VPd_3$ (space group $I4/mmm$, $\Delta H_f$ = 5 meV/atom) |
| $InSr_3$ | aflow:e7ed70c4711eb718 | $P4/mmm$, No. 123 | 35% | composition not found, nearest are $Sr_{28}In_{11}$ (space group $Imm2$) and Sr (space group $Fm\bar{3}m$) |
| $CoNb_2$ | aflow:f5cc5eaf65e692a9 | $I4/mcm$, No. 140 | 35% | composition not found, nearest are $Nb_{6.7}Co_{6.3}$ (space group $R\bar{3}m$, POCC structure) and $Nb_{0.77}Co_{0.23}$ (space group $Fm\bar{3}m$, POCC structure) |
| $Ag_3In_2$ | aflow:6ee057decaf093d0 | $Fdd2$, No. 43 | 34% | composition not found, nearest are $Ag_9In_4$ (space group $P\bar{4}3m$, $\Delta H_f$ = 21 meV/atom) and $AgIn_2$ (space group $I4/mcm$, $\Delta H_f$ = 53 meV/atom) |
| AgPt | aflow:360240dae753fec6 | $P\bar{6}m2$, No. 187 | 34% | polymorph found (space group $Fm\bar{3}m$, POCC structure) |
| $OsY_3$ | aflow:bd3056780447faf0 | $Pnma$, No. 62 | 34% | composition found, one-to-one match |
| $RuZn_6$ | aflow:96142e32718a5ee0 | $P4_132$, No. 213 | 33% | composition found, one-to-one match |
| $Ag_2Zn$ | aflow:1ba6b4b5c0ed9788 | $P\bar{6}2m$, No. 189 | 33% | composition not found, nearest Ag (space group $Fm\bar{3}m$) and $Ag_{4.5}Zn_{4.5}$ (space group $P\bar{3}$, POCC structure) |
| MnRh | aflow:87d6637b32224f7b | $Pm\bar{3}m$, No. 221 | 32% | polymorph found (space group $P4/mmm$, $\Delta H_f$ = 156 meV/atom) |
| $AgNa_2$ | aflow:f08f2f61de18aa61 | $I4/mcm$, No. 140 | 32% | composition not found, nearest are $NaAg_2$ (space group $Fd\bar{3}m$, $\Delta H_f$ = 208 meV/atom) and Na (space group $R\bar{3}m$) |
| $BeRe_2$ | aflow:7ce4fcc3660c16cf | $I4/mcm$, No. 140 | 31% | composition not found, nearest are $Be_2Re$ (space group $P6_3/mmc$) and Re (space group $P6_3/mmc$) |
| $As_2Tc$† | aflow:e94ab366799a008c | $C2/m$, No. 12 | 30% | no diagram |
| $Be_2Mn$† | aflow:eec0d7b6b0d1dfa0 | $P6_3/mmc$, No. 194 | 30% | no diagram |
| AgAu | aflow:6f3f5b696f5aa391 | $P4/mmm$, No. 123 | 29% | polymorph found (space group $Fm\bar{3}m$, POCC structure) |
| $Nb_5Re_{24}$ | aflow:ca051dbe25c55b92 | $I\bar{4}3m$, No. 217 | 29% | composition not found, nearest are $Nb_{0.25}Re_{0.75}$ (space group $I\bar{4}3m$, POCC structure) and $Nb_{0.01}Re_{0.99}$ (space group $P6_3/mmc$, POCC structure) |
| $La_3Os$† | aflow:a9daa69940d3a59a | $Pnma$, No. 62 | 28% | no diagram |
| $Be_5Pt$ | aflow:8ce84acfd6f9ea44 | $F\bar{4}3m$, No. 216 | 28% | composition found, one-to-one match |
| $Ir_8Ru$ | aflow:487f7cf6c3fb13f0 | $I4/mmm$, No. 139 | 27% | composition not found, nearest are Ir (space group $Fm\bar{3}m$) and $Ru_{0.3}Ir_{0.7}$ (space group $Fm\bar{3}m$, POCC structure) |
| InK | aflow:66af8171e22dc212 | $R\bar{3}m$, No. 166 | 27% | composition not found, nearest are $K_8In_{11}$ (space group $R\bar{3}c$) and K (space group $Im\bar{3}m$) |

[a]Phases with equivalent structures in the AFLOW ICSD catalog are excluded. The list is sorted by the absolute value ratio between the stability criterion ($\delta_{sc}$) and the formation enthalpy ($H_f$) (shown as a percentage). POCC denotes a partially occupied (disordered) structure.[40] Comparisons with the ASM database include phases that are observed at high temperatures and pressures. [b]The superscripted dagger symbol (†) indicates that no binary phase diagram is available on the ASM Alloy Phase Diagram database.[5]

In the illustrations, color is used to differentiate points with different enthalpies and indicate depth of the facets (three dimensions). The report includes entry-specific data from the AFLOW.org database (prototype, auid, original and relaxed space groups, spin, formation enthalpy $H_f$, and entropic temperature $T_S$) as well as calculated thermodynamic data (distance to the hull $\Delta H_f$, the balanced decomposition reaction for unstable phases, the stability criterion $\delta_{sc}$ for stable phases, and phases in coexistence). Stable phases (and those that are structurally equivalent) are highlighted in green, and similar phases (comparing relaxed space groups) are highlighted in orange. Links are also incorporated in the report, including external hyperlinks to entry pages on AFLOW.org (see prototypes) and internal links to relevant parts of the report (see decomposition reaction and *N*-phase equilibria). Internal links are also included on the convex hull illustration (see the Supporting Information). The information is provided in the form of plain text and JSON files. Keys and format are explained in the Supporting Information.

**3.2. Web Application.** A modern web application has been developed to provide an enhanced, command-line-free platform for AFLOW-CHULL. The project includes a rich feature set consisting of binary and ternary convex hull visualizations, AFLOW.org entry data retrieval, and a convex hull comparison interface. The application is divided into four components: the periodic table, the visualization viewport, the selected entries list, and the comparison page.

The periodic table component is initially displayed. Hulls can be queried by selecting/typing in the elemental combination. As elements are added to the search, the periodic table reacts to the query depending on the reliability of the hull: green (fully reliable, $N_{entries} \geq 200$), orange (potentially reliable, $100 \leq N_{entries} < 200$), red (unreliable, $N_{entries} < 100$), and gray (unavailable, $N_{entries} = 0$). Each new hull request triggers a fresh data download and analysis, offering the most up-to-date results given that new calculations are injected into the AFLOW.org repository daily. Once the analysis is performed and results are retrieved, the application loads the visualization viewport prompting a redirect to the URL end point of the selected hull, e.g., /hull/AlHfNi. The URL is ubiquitous and can be shared/cited.

When a binary convex hull is selected, the viewport reveals a traditional two-dimensional plot (Figure 6a), while a ternary hull yields a three-dimensional visualization (Figure 6b). The scales



DOI: 10.1021/acs.jcim.8b00393
J. Chem. Inf. Model. 2018, 58, 2477−2490

**Table 2. Listing of the 25 Ternary Phases Predicted to Be Most Stable by AFLOW-CHULL[a]**

| compound[b] | auid | relaxed space group | $\lvert\delta_{sc}/H_f\rvert$ | comparison with ASM Alloy Phase Diagrams[5] |
|---|---|---|---|---|
| $MgSe_2Zn_2$† | aflow:df0cdf0f1ad3110d | *Fmmm*, No. 69 | 58% | no diagram, two of three binary phase diagrams found (no Mg−Se) |
| $Be_4OsTi$† | aflow:8c51c7ab71f25d11 | $F\bar{4}3m$, No. 216 | 38% | no diagram, two of three binary phase diagrams found (no Be−Os) |
| $Be_4OsV$† | aflow:4e5711451dc4b601 | $F\bar{4}3m$, No. 216 | 38% | no diagram, two of three binary phase diagrams found (no Be−Os) |
| $Ag_2InZr$ | aflow:1684c02e75b0d950 | $Fm\bar{3}m$, No. 225 | 35% | composition not found, nearest are $Ag_{0.8}In_{0.2}$ (space group $Fm\bar{3}m$, POCC structure), $Zr_{0.5}In_{0.5}$ (space group $Fm\bar{3}m$, POCC structure), and $AgZr_5In_3$ (space group $P6_3/mcm$) |
| $Be_4RuTi$†‡ | aflow:b85addbb42c47ae9 | $F\bar{4}3m$, No. 216 | 32% | no diagram, all three binary phase diagrams found |
| $Be_4FeTi$†‡ | aflow:cabd6decf5b6c991 | $F\bar{4}3m$, No. 216 | 29% | no diagram, all three binary phase diagrams found |
| $Be_4ReV$†‡ | aflow:7010472778d429f7 | $F\bar{4}3m$, No. 216 | 29% | no diagram, all three binary phase diagrams found |
| $Ba_2RhZn$† | aflow:e4cc9eea02d9d303 | *Cm*, No. 8 | 29% | no diagram, two of three binary phase diagrams found (no Ba−Rh) |
| $Be_4HfOs$† | aflow:2ace5c5383f8ea10 | $F\bar{4}3m$, No. 216 | 27% | no diagram, two of three binary phase diagrams found (no Be−Os) |
| $Be_4ReTi$†‡ | aflow:de79192a0c4e751f | $F\bar{4}3m$, No. 216 | 27% | no diagram, all three binary phase diagrams found |
| $Be_4TcV$† | aflow:d484b95ba623f9f7 | $F\bar{4}3m$, No. 216 | 27% | no diagram, two of three binary phase diagrams found (no Be−Tc) |
| $Be_4TcTi$† | aflow:c13660b990eb9570 | $F\bar{4}3m$, No. 216 | 27% | no diagram, two of three binary phase diagrams found (no Be−Tc) |
| $Be_4RuV$†‡ | aflow:07840d9e13694f7e | $F\bar{4}3m$, No. 216 | 27% | no diagram, all three binary phase diagrams found |
| $AsCoTi$†‡ | aflow:5778f3b725d5f850 | $F\bar{4}3m$, No. 216 | 26% | no diagram, all three binary phase diagrams found |
| $Be_4MnTi$† | aflow:9a10dd8a8224e158 | $F\bar{4}3m$, No. 216 | 26% | no diagram, two of three binary phase diagrams found (no Be−Mn) |
| $Be_4OsZr$† | aflow:de412213bdefbd14 | $F\bar{4}3m$, No. 216 | 26% | no diagram, two of three binary phase diagrams found (no Be−Os) |
| $Be_4IrTi$† | aflow:07bcc161f57da109 | $F\bar{4}3m$, No. 216 | 26% | no diagram, two of three binary phase diagrams found (no Be−Ir) |
| $Mg_2ScTl$† | aflow:90b98cdcd6eea146 | *P4/mmm*, No. 123 | 25% | no diagram, two of three binary phase diagrams found (no Sc−Tl) |
| $Be_4MnV$† | aflow:086b4a89f8d62804 | $F\bar{4}3m$, No. 216 | 25% | no diagram, two of three binary phase diagrams found (no Be−Mn) |
| $AuBe_4Cu$†‡ | aflow:0595e3d45678a85c | $F\bar{4}3m$, No. 216 | 25% | no diagram, all three binary phase diagrams found |
| $BiRhZr$†‡ | aflow:d7fed8d4996290f4 | $F\bar{4}3m$, No. 216 | 24% | no diagram, all three binary phase diagrams found |
| $LiMg_2Zn$ | aflow:80bf8ad33a5bb33b | $Fm\bar{3}m$, No. 225 | 21% | composition not found, nearest are Li (space group $Im\bar{3}m$, $\Delta H_f = 2$ meV/atom), Mg (space group $P6_3/mmc$), and $Li_{0.77}MgZn_{1.23}$ (space group $Fd\bar{3}m$, POCC structure) |
| $Be_4RhTi$† | aflow:faa814b1222e8aea | $F\bar{4}3m$, No. 216 | 21% | no diagram, two of three binary phase diagrams found (no Be−Rh) |
| $AuCu_4Hf$†‡ | aflow:26cc4fc55644b0d8 | $F\bar{4}3m$, No. 216 | 21% | no diagram, all three binary phase diagrams found |
| $Mg_2SeZn_2$† | aflow:ab57b1ae74f4c6d4 | *Fmmm*, No. 69 | 21% | no diagram, two of three binary phase diagrams found (no Mg−Se) |

[a]Phases with equivalent structures in the AFLOW ICSD catalog are excluded. The list is sorted by the absolute value ratio between the stability criterion ($\delta_{sc}$) and the formation enthalpy ($H_f$) (shown as a percentage). POCC denotes a partially occupied (disordered) structure.[40] Comparisons with the ASM database include phases that are observed at high temperatures and pressures. [b]The superscripted dagger symbol (†) indicates no ternary phase diagram is available on the ASM Alloy Phase Diagram database,[5] while the superscripted double dagger symbol (‡) indicates that all three relevant binaries are available.

of both are tunable, and the three-dimensional visualization offers mouse-enabled pan and zoom.

Common to both types is the ability to select and highlight points. When a point is selected, its name will appear within the sidebar. The information component is populated with a grid of cards containing properties of each selected point (entry), including a link to the AFLOW.org entry page (see Figure 6c).

The application environment stores all previously selected hulls, which are retrievable via the hull comparison component (see Figure 6d). On this page, each hull visualization is displayed as a card on a grid. This grid serves as both a history and a means to compare hulls.

**3.3. Candidates for Synthesis.** To demonstrate the capability of AFLOW-CHULL, all binary and ternary systems in the AFLOW.org repository are explored for ones yielding well-converged thermodynamic properties. Since reliability constraints are built-in, no prefiltering is required and all potential elemental combinations are attempted. Across all catalogs present in the database, there exist materials composed of 86 elements, including H, He, Li, Be, B, C, N, O, F, Ne, Na, Mg, Al, Si, P, S, Cl, Ar, K, Ca, Sc, Ti, V, Cr, Mn, Fe, Co, Ni, Cu, Zn, Ga, Ge, As, Se, Br, Kr, Rb, Sr, Y, Zr, Nb, Mo, Tc, Ru, Rh, Pd, Ag, Cd, In, Sn, Sb, Te, I, Xe, Cs, Ba, La, Ce, Pr, Nd, Pm, Sm, Eu, Gd, Tb, Dy, Ho, Er, Tm, Yb, Lu, Hf, Ta, W, Re, Os, Ir, Pt, Au, Hg, Tl, Pb, Bi, Ac, Th, and Pa. Hulls are eliminated if (i) systems are unreliable based on count (fewer than 200 entries among binary combinations), and (ii) systems show significant immiscibility (fewer than 50 points below the zero $H_f$ tie-line). Ternary systems are further screened for those containing ternary ground-state structures. The analysis resulted in the full thermodynamic characterization of 493 binary and 873 ternary systems. The results are provided in the Supporting Information.

Leveraging the JSON outputs, reliable hulls are further explored for new stable phases. Phases are first screened (eliminated) if an equivalent structure exists in the AFLOW.org ICSD catalog, and candidates are sorted by their relative stability criterion, i.e., $\lvert\delta_{sc}/H_f\rvert$. This dimensionless quantity captures the effect of the phase on the minimum energy surface, relative to its depth, enabling comparisons across hulls. An example Python script that performs this analysis is provided in the Supporting Information.

The top 25 most stable binary and ternary phases are presented in Tables 1 and 2, respectively, for which extended analysis is performed based on information stored in the ASM (American Society for Metals) Alloy Phase Diagram database.[5] The ASM database is the largest of its type, aggregating a wealth of experimental phase diagram information: 40 300 binary and ternary alloy phase diagrams from over 9000 systems. Upon searching the ASM Web site, many binary systems from Table 1 are unavailable and denoted by a superscripted dagger symbol (†). Among those that are available, some stable phases have already been observed, including $OsY_3$, $RuZn_6$, and $Be_5Pt$. For AgPt, MnRh, and AgAu, the composition is successfully predicted, but polymorphs (structurally distinct phases) are observed instead. For all other phases on the list, the composition has not been observed. The discrepancy may be isolated to the


DOI: 10.1021/acs.jcim.8b00393
J. Chem. Inf. Model. 2018, 58, 2477−2490

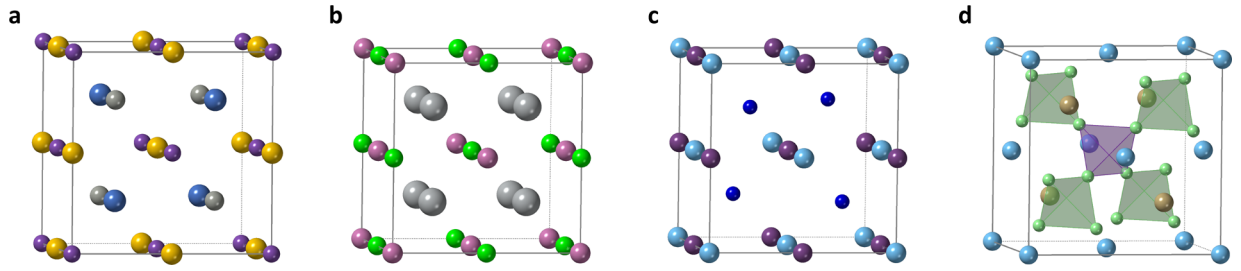


**Figure 7.** Illustration of the most prevalent stable ternary structures. (a) The conventional cubic cell of the "quaternary-Heusler" structure, LiMgPdSn.[78,79] Each species occupies a Wyckoff site of space group $F\bar{4}3m$, No. 216: Sn (purple) (4a), Mg (yellow) (4b), Pd (gray) (4c), and Li (blue) (4d). (b) The conventional cubic cell of the Heusler structure, represented here by $Ag_2InZr$. Each species occupies a Wyckoff site of space group $Fm\bar{3}m$, No. 225: In (pink) (4a), Zr (green) (4b), Ag (light gray) (8c). (c) The conventional cubic cell of the half-Heusler $C1_b$ structure, represented here by AsCoTi. Each species occupies a Wyckoff site of space group $F\bar{4}3m$, No. 216: Ti (light blue) (4a), As (purple) (4b), Co (dark blue) (4c). The (4d) site is empty. (d) The conventional cubic cell of the $C15_b$-type crystal, here represented by $Be_4OsTi$. Each species occupies a Wyckoff site of space group $F\bar{4}3m$, No. 216: Ti (light blue) (4a), Os (brown) (4c), and Be (light green) (8e). The (4d) site is empty, and the Be atoms form a tetrahedron centered around the (4b) site depicted in panel (a).

phase, or indicative of a more extreme contradiction in the topology of the hull, and thus, nearby phases are also analyzed. For the Be−Re system, although $BeRe_2$ has not been observed, both $Be_2Re$ and Re are successfully identified. Most of the remaining phases show the nearest phase to be a disordered (partially occupied) structure, which are excluded from the AFLOW.org repository. Addressing disorder is a particularly challenging task in ab initio studies. However, recent high-throughput techniques[40] show promise for future investigations and will be integrated in future releases of the code.

Among the most stable ternary phases, only two systems have phase diagrams available in the ASM database: Ag−In−Zr and Li−Mg−Zn. For the Ag−In−Zr system, the composition of $Ag_2InZr$ is not observed and the nearest stable phases include disordered structures and $AgZr_5In_3$, which has not yet been included the AFLOW.org repository. For Li−Mg−Zn, the composition of $LiMg_2Zn$ is also not observed and the nearest stable phases include unaries Li, Mg, and a disordered structure. All other ternary systems are entirely unexplored. Ternary phases with all three binary phase diagrams available are denoted with a superscripted double dagger symbol (‡), suggesting experimental feasibility.

A striking feature of Table 2 is that most of the stable structures are found to be in space group $F\bar{4}3m$, No. 216. This structure has a face-centered cubic lattice with symmetry operations that include a 4-fold rotation about the ⟨001⟩ axes, a 3-fold rotation about the ⟨111⟩ axes, and no inversion. Further study reveals that these phases, as well as $Fm\bar{3}m$, No. 225 $Ag_2InZr$ and $LiMg_2Zn$, can be obtained from the "quaternary-Heusler" structure, LiMgPdSn[78,79] (see Figure 7a). The prototype can be considered a $2\times2\times2$ supercell of the body-centered cubic structure. The Sn, Mg, Au, and Li atoms all occupy different Wyckoff positions of space group $F\bar{4}3m$ and each atom has two sets of nearest neighbors, each 4-fold coordinated. Various decorations of these Wyckoff positions generate the other structures:

- By decorating two second-neighbor atom sites identically, a Heusler alloy forms (*Strukturbericht* symbol $L2_1$).[43,80] For example, the following substitutions generate $Ag_2InZr$ (Figure 7b): Pd → Ag, Li → Ag, Sn → In, and Mg → Zr. Since the crystal now has an inversion center, the space group becomes $Fm\bar{3}m$, No. 225. As in LiMgPdSn, each atom has two sets of 4-fold coordinated nearest neighbors, each arranged as a tetrahedron. Now, however, one species (Ag) has second-nearest neighbors of the same type.
- By removing the Li atom completely, a half-Heusler forms ($C1_b$).[43,81] There are two half-Heusler systems in Table 2: AsCoTi (Figure 7c) and BiRhZr. The structure does differ from that of LiMgPdSn and $L2_1$, as the Ag and Ti atoms are 4-fold coordinated, with only Co having the coordination seen in the previous structures.
- The majority of structures in Table 2 are type $C15_b$, prototype $AuBe_5$[43,82] (AFLOW prototype: AB5_cF24_216_a_ce[83]), represented by $Be_4OsTi$, shown in Figure 7d. Compared to the $C1_b$, $C15_b$ contains an (8e) Wyckoff position forming a tetrahedra centered around the (4b) Wyckoff position. Replacing the tetrahedra with a single atom returns the $C1_b$ structure.

Hence, of the 25 most stable ternary structures, 21 are of related structure.

Sampling bias likely plays a role in the high prominence of space group $F\bar{4}3m$ #216 structures in Table 2, but cannot fully account for the anomaly. Space group $F\bar{4}3m$, No. 216 constitutes ∼17% of the LIB3 catalog, which contains the bulk of the AFLOW.org repository (at over 1.4 million ternary systems) generated largely by small structure prototypes. For context, space group $F\bar{4}3m$, No. 216 is ranked ∼20th of the most common space groups in the ICSD,[84] appearing in ∼1% of all entries. Further exploration of larger structure ternary prototypes covering the full range of space groups is needed to fully elucidate the nature of this structure's stability.

The regular-, inverse-, and half-Heusler prototypes were added to LIB3 for the exploration of new magnets, of which two were discovered.[4] The Heusler set includes more than 236 000 structures, most of which remains unexplored. The fully sorted lists of stable binary and ternary phases are presented in the Supporting Information.

## 4. CONCLUSIONS

Thermodynamic analysis is a critical step for any effective materials design workflow. Being a collective characterization, thermodynamics requires comparisons between many configurations of the system. The availability of large databases[8−15] allows the construction of computationally based phase diagrams. AFLOW-CHULL presents a complete software infrastructure, including flexible protocols for data retrieval, analysis, and verification.[12,44] The module is exhaustively applied to the AFLOW.org repository and identified several new candidate phases: 17 promising $C15_b$-type structures and two half-Heuslers. The extension of AFLOW-CHULL to repositories



DOI: 10.1021/acs.jcim.8b00393
J. Chem. Inf. Model. 2018, 58, 2477−2490

beyond AFLOW.org can be performed by adapting the open-source C++ code and/or Python module. Computational platforms such as AFLOW-CHULL are valuable tools for guiding synthesis, including high-throughput and even autonomous approaches.[85−88]

## ■ ASSOCIATED CONTENT

### Supporting Information

The Supporting Information is available free of charge on the ACS Publications website at DOI: 10.1021/acs.jcim.8b00393.

An AFLOW-CHULL manual, including example scripts illustrating how to employ AFLOW-CHULL from within a Python environment (PDF)

A snapshot (inventory) of binary and ternary alloy systems available in the AFLOW.org repository, and the full list of stable phases ranked by their relative stability criterion (PDF)

Thermodynamic characterization of 493 binary systems (PDF)

Ternary systems Ag-Al-Ca−Au-Pd-Y (Part 1 of 3) (PDF)

Ternary systems Au-Pd-Zn−In-Mg-Ni (Part 2 of 3) (PDF)

Ternary systems In-Mg-Pd−Te-Tl-Y (Part 3 of 3) (PDF)

## ■ AUTHOR INFORMATION


### Corresponding Author

*E-mail: stefano@duke.edu.

### ORCID

Corey Oses: 0000-0002-3790-1377

Stefano Curtarolo: 0000-0003-0570-8238


### Notes

The authors declare no competing financial interest.

## ■ ACKNOWLEDGMENTS

We thank Drs. G. L. W. Hart, D. Usanmaz, R. Friedrich, M. Esters, P. Nath, D. Ford, P. Colinet, O. Isayev, A. Tropsha, N. Mingo, J. Carrete, and L. M. Ghiringhelli for insightful discussions. Research sponsored by the Department of Defense (ONR: Nos. N00014-17-1-2090, N00014-16-1-2583, N00014-16-1-2326, N00014-14-1-0526), and the National Science Foundation (under DMREF Grant No. DMR-1436151). C.O. acknowledges support from the National Science Foundation Graduate Research Fellowship (under Grant No. DGF1106401). D.H. acknowledges support from the Department of Defense through the National Defense Science and Engineering Graduate (NDSEG) Fellowship Program. S.C. acknowledges the Alexander von Humboldt-Foundation for financial support.

## ■ REFERENCES


(1) Jansen, M. A. Concept for Synthesis Planning in Solid-State Chemistry. *Angew. Chem., Int. Ed.* **2002**, *41*, 3746−3766.

(2) Potyrailo, R.; Rajan, K.; Stoewe, K.; Takeuchi, I.; Chisholm, B.; Lam, H. Combinatorial and high-throughput screening of materials libraries: Review of state of the art. *ACS Comb. Sci.* **2011**, *13*, 579−633.

(3) Kuz'min, M. D.; Skokov, K. P.; Jian, H.; Radulov, I.; Gutfleisch, O. Towards high-performance permanent magnets without rare earths. *J. Phys.: Condens. Matter* **2014**, *26*, 064205.

(4) Sanvito, S.; Oses, C.; Xue, J.; Tiwari, A.; Zic, M.; Archer, T.; Tozman, P.; Venkatesan, M.; Coey, J. M. D.; Curtarolo, S. Accelerated discovery of new magnets in the Heusler alloy family. *Sci. Adv.* **2017**, *3*, e1602241.

(5) Villars, P.; Okamoto, H.; Cenzual, K. *ASM Alloy Phase Diagram Database*. Available via the Internet at: http://www1.asminternational.org/AsmEnterprise/APD (accessed Aug. 13, 2018).

(6) Walsh, A. Inorganic materials: The quest for new functionality. *Nat. Chem.* **2015**, *7*, 274−275.

(7) Isayev, O.; Oses, C.; Toher, C.; Gossett, E.; Curtarolo, S.; Tropsha, A. Universal fragment descriptors for predicting electronic properties of inorganic crystals. *Nat. Commun.* **2017**, *8*, 15679.

(8) Curtarolo, S.; Setyawan, W.; Wang, S.; Xue, J.; Yang, K.; Taylor, R. H.; Nelson, L. J.; Hart, G. L. W.; Sanvito, S.; Buongiorno Nardelli, M.; Mingo, N.; Levy, O. AFLOWLIB.ORG: A distributed materials properties repository from high-throughput *ab initio* calculations. *Comput. Mater. Sci.* **2012**, *58*, 227−235.

(9) Taylor, R. H.; Rose, F.; Toher, C.; Levy, O.; Yang, K.; Buongiorno Nardelli, M.; Curtarolo, S. A RESTful API for exchanging materials data in the AFLOWLIB.org consortium. *Comput. Mater. Sci.* **2014**, *93*, 178−192.

(10) Calderon, C. E.; Plata, J. J.; Toher, C.; Oses, C.; Levy, O.; Fornari, M.; Natan, A.; Mehl, M. J.; Hart, G. L. W.; Buongiorno Nardelli, M.; Curtarolo, S. The AFLOW standard for high-throughput materials science calculations. *Comput. Mater. Sci.* **2015**, *108*, 233−238.

(11) Rose, F.; Toher, C.; Gossett, E.; Oses, C.; Buongiorno Nardelli, M.; Fornari, M.; Curtarolo, S. AFLUX: The LUX materials search API for the AFLOW data repositories. *Comput. Mater. Sci.* **2017**, *137*, 362−370.

(12) Scheffler, M.; Draxl, C.; Computer Center of the Max-Planck Society, Garching. *The NoMaD Repository*. Available via the Internet at: http://nomad-repository.eu (accessed Aug. 13, 2018).

(13) Jain, A.; Ong, S. P.; Hautier, G.; Chen, W.; Richards, W. D.; Dacek, S.; Cholia, S.; Gunter, D.; Skinner, D.; Ceder, G.; Persson, K. A. Commentary: The Materials Project: A materials genome approach to accelerating materials innovation. *APL Mater.* **2013**, *1*, 011002.

(14) Saal, J. E.; Kirklin, S.; Aykol, M.; Meredig, B.; Wolverton, C. Materials Design and Discovery with High-Throughput Density Functional Theory: The Open Quantum Materials Database (OQMD). *JOM* **2013**, *65*, 1501−1509.

(15) Landis, D. D.; Hummelshøj, J. S.; Nestorov, S.; Greeley, J.; Dułak, M.; Bligaard, T.; Nørskov, J. K.; Jacobsen, K. W. The Computational Materials Repository. *Comput. Sci. Eng.* **2012**, *14*, 51−57.

(16) Pizzi, G.; Cepellotti, A.; Sabatini, R.; Marzari, N.; Kozinsky, B. AiiDA: automated interactive infrastructure and database for computational science. *Comput. Mater. Sci.* **2016**, *111*, 218−230.

(17) Nyshadham, C.; Oses, C.; Hansen, J. E.; Takeuchi, I.; Curtarolo, S.; Hart, G. L. W. A computational high-throughput search for new ternary superalloys. *Acta Mater.* **2017**, *122*, 438−447.

(18) Bechtel, J. S.; Van der Ven, A. First-principles thermodynamics study of phase stability in inorganic halide perovskite solid solutions. *Phys. Rev. Mater.* **2018**, *2*, 045401.

(19) Li, W.; Jacobs, R.; Morgan, D. Predicting the thermodynamic stability of perovskite oxides using machine learning models. *Comput. Mater. Sci.* **2018**, *150*, 454−463.

(20) Balachandran, P. V.; Emery, A. A.; Gubernatis, J. E.; Lookman, T.; Wolverton, C.; Zunger, A. Predictions of new $ABO_3$ perovskite compounds by combining machine learning and density functional theory. *Phys. Rev. Mater.* **2018**, *2*, 043802.

(21) Levy, O.; Hart, G. L. W.; Curtarolo, S. Uncovering Compounds by Synergy of Cluster Expansion and High-Throughput Methods. *J. Am. Chem. Soc.* **2010**, *132*, 4830−4833.

(22) Levy, O.; Hart, G. L. W.; Curtarolo, S. Hafnium binary alloys from experiments and first principles. *Acta Mater.* **2010**, *58*, 2887−2897.

(23) Levy, O.; Chepulskii, R. V.; Hart, G. L. W.; Curtarolo, S. The New Face of Rhodium Alloys: Revealing Ordered Structures from First Principles. *J. Am. Chem. Soc.* **2010**, *132*, 833−837.

(24) Levy, O.; Hart, G. L. W.; Curtarolo, S. Structure maps for hcp metals from first-principles calculations. *Phys. Rev. B: Condens. Matter Mater. Phys.* **2010**, *81*, 174106.

(25) Levy, O.; Jahnátek, M.; Chepulskii, R. V.; Hart, G. L. W.; Curtarolo, S. Ordered Structures in Rhenium Binary Alloys from First-Principles Calculations. *J. Am. Chem. Soc.* **2011**, *133*, 158−163.

(26) Jahnátek, M.; Levy, O.; Hart, G. L. W.; Nelson, L. J.; Chepulskii, R. V.; Xue, J.; Curtarolo, S. Ordered phases in ruthenium binary alloys from high-throughput first-principles calculations. *Phys. Rev. B: Condens. Matter Mater. Phys.* **2011**, *84*, 214110.
(27) Levy, O.; Xue, J.; Wang, S.; Hart, G. L. W.; Curtarolo, S. Stable ordered structures of binary technetium alloys from first principles. *Phys. Rev. B: Condens. Matter Mater. Phys.* **2012**, *85*, 012201.
(28) Bloch, J.; Levy, O.; Pejova, B.; Jacob, J.; Curtarolo, S.; Hjörvarsson, B. Prediction and Hydrogen Acceleration of Ordering in Iron-Vanadium Alloys. *Phys. Rev. Lett.* **2012**, *108*, 215503.
(29) Hart, G. L. W.; Curtarolo, S.; Massalski, T. B.; Levy, O. Comprehensive Search for New Phases and Compounds in Binary Alloy Systems Based on Platinum-Group Metals, Using a Computational First-Principles Approach. *Phys. Rev. X* **2013**, *3*, 041035.
(30) Barzilai, S.; Toher, C.; Curtarolo, S.; Levy, O. Evaluation of the tantalum-titanium phase diagram from *ab-initio* calculations. *Acta Mater.* **2016**, *120*, 255−263.
(31) Perim, E.; Lee, D.; Liu, Y.; Toher, C.; Gong, P.; Li, Y.; Simmons, W. N.; Levy, O.; Vlassak, J. J.; Schroers, J.; Curtarolo, S. Spectral descriptors for bulk metallic glasses based on the thermodynamics of competing crystalline phases. *Nat. Commun.* **2016**, *7*, 12315.
(32) Barzilai, S.; Toher, C.; Curtarolo, S.; Levy, O. The effect of lattice stability determination on the computational phase diagrams of intermetallic alloys. *J. Alloys Compd.* **2017**, *728*, 314−321.
(33) Barzilai, S.; Toher, C.; Curtarolo, S.; Levy, O. Molybdenum-titanium phase diagram evaluated from *ab initio* calculations. *Phys. Rev. Mater.* **2017**, *1*, 023604.
(34) Hever, A.; Oses, C.; Curtarolo, S.; Levy, O.; Natan, A. The Structure and Composition Statistics of 6A Binary and Ternary Crystalline Materials. *Inorg. Chem.* **2018**, *57*, 653−667.
(35) Rost, C. M.; Sachet, E.; Borman, T.; Moballegh, A.; Dickey, E. C.; Hou, D.; Jones, J. L.; Curtarolo, S.; Maria, J.-P. Entropy-stabilized oxides. *Nat. Commun.* **2015**, *6*, 8485.
(36) Rak, Z.; Rost, C. M.; Lim, M.; Sarker, P.; Toher, C.; Curtarolo, S.; Maria, J.-P.; Brenner, D. W. Charge compensation and electrostatic transferability in three entropy-stabilized oxides: Results from density functional theory calculations. *J. Appl. Phys.* **2016**, *120*, 095105.
(37) Lederer, Y.; Toher, C.; Vecchio, K. S.; Curtarolo, S. The search for high entropy alloys: a high-throughput ab-initio approach. *Acta Mater.* **2018**, *159*, 364−383.
(38) *GNU General Public License*. Available via the Internet at: http://www.gnu.org/licenses (accessed Aug. 13, 2018).
(39) Curtarolo, S.; Setyawan, W.; Hart, G. L. W.; Jahnátek, M.; Chepulskii, R. V.; Taylor, R. H.; Wang, S.; Xue, J.; Yang, K.; Levy, O.; Mehl, M. J.; Stokes, H. T.; Demchenko, D. O.; Morgan, D. AFLOW: An automatic framework for high-throughput materials discovery. *Comput. Mater. Sci.* **2012**, *58*, 218−226.
(40) Yang, K.; Oses, C.; Curtarolo, S. Modeling Off-Stoichiometry Materials with a High-Throughput *Ab-Initio* Approach. *Chem. Mater.* **2016**, *28*, 6484−6492.
(41) Carrete, J.; Mingo, N.; Wang, S.; Curtarolo, S. Nanograined Half-Heusler Semiconductors as Advanced Thermoelectrics: An Ab Initio High-Throughput Statistical Study. *Adv. Funct. Mater.* **2014**, *24*, 7427−7432.
(42) Setyawan, W.; Curtarolo, S. High-throughput electronic band structure calculations: Challenges and tools. *Comput. Mater. Sci.* **2010**, *49*, 299−312.
(43) Mehl, M. J.; Hicks, D.; Toher, C.; Levy, O.; Hanson, R. M.; Hart, G. L. W.; Curtarolo, S. The AFLOW Library of Crystallographic Prototypes: Part 1. *Comput. Mater. Sci.* **2017**, *136*, S1−S828.
(44) Supka, A. R.; Lyons, T. E.; Liyanage, L. S. I.; D'Amico, P.; Al Rahal Al Orabi, R.; Mahatara, S.; Gopal, P.; Toher, C.; Ceresoli, D.; Calzolari, A.; Curtarolo, S.; Buongiorno Nardelli, M.; Fornari, M. AFLOW$\pi$: A minimalist approach to high-throughput *ab initio* calculations including the generation of tight-binding hamiltonians. *Comput. Mater. Sci.* **2017**, *136*, 76−84.
(45) Hicks, D.; Oses, C.; Gossett, E.; Gomez, G.; Taylor, R. H.; Toher, C.; Mehl, M. J.; Levy, O.; Curtarolo, S. *AFLOW-SYM*: platform for the complete, automatic and self-consistent symmetry analysis of crystals. *Acta Crystallogr., Sect. A: Found. Adv.* **2018**, *74*, 184−203.
(46) Rohrer, G. S.; Affatigato, M.; Backhaus, M.; Bordia, R. K.; Chan, H. M.; Curtarolo, S.; Demkov, A.; Eckstein, J. N.; Faber, K. T.; Garay, J. E.; Gogotsi, Y.; Huang, L.; Jones, L. E.; Kalinin, S. V.; Lad, R. J.; Levi, C. G.; Levy, J.; Maria, J.-P.; Mattos, L., Jr.; Navrotsky, A.; Orlovskaya, N.; Pantano, C.; Stebbins, J. F.; Sudarshan, T. S.; Tani, T.; Weil, K. S. Challenges in Ceramic Science: A Report from the Workshop on Emerging Research Areas in Ceramic Science. *J. Am. Ceram. Soc.* **2012**, *95*, 3699−3712.
(47) Barber, C. B.; Dobkin, D. P.; Huhdanpaa, H. The quickhull algorithm for convex hulls. *ACM Trans. Math. Soft.* **1996**, *22*, 469−483.
(48) Yong, J.; Jiang, Y.; Usanmaz, D.; Curtarolo, S.; Zhang, X.; Li, L.; Pan, X.; Shin, J.; Takeuchi, I.; Greene, R. L. Robust Topological Surface State of Kondo insulator $SmB_6$ Thin Films. *Appl. Phys. Lett.* **2014**, *105*, 222403.
(49) Toher, C.; Plata, J. J.; Levy, O.; de Jong, M.; Asta, M. D.; Buongiorno Nardelli, M.; Curtarolo, S. High-throughput computational screening of thermal conductivity, Debye temperature, and Grüneisen parameter using a quasiharmonic Debye model. *Phys. Rev. B: Condens. Matter Mater. Phys.* **2014**, *90*, 174107.
(50) Nath, P.; Plata, J. J.; Usanmaz, D.; Al Rahal Al Orabi, R.; Fornari, M.; Buongiorno Nardelli, M.; Toher, C.; Curtarolo, S. High-Throughput Prediction of Finite-Temperature Properties using the Quasi-Harmonic Approximation. *Comput. Mater. Sci.* **2016**, *125*, 82−91.
(51) Majzoub, E. H.; McCarty, K. F.; Ozoliņš, V. Lattice dynamics of $NaAlH_4$ from high-temperature single-crystal Raman scattering and ab initio calculations: Evidence of highly stable $AlH_4^-$ anions. *Phys. Rev. B: Condens. Matter Mater. Phys.* **2005**, *71*, 024118.
(52) The formation enthalpy is not to be confused with the cohesive energy, which quantifies the energy difference between the phase and its fully gaseous (single atoms) counterpart, i.e., the energy in all bonds.
(53) Wang, L.; Maxisch, T.; Ceder, G. Oxidation energies of transition metal oxides within the GGA+U framework. *Phys. Rev. B: Condens. Matter Mater. Phys.* **2006**, *73*, 195107.
(54) Stevanović, V.; Lany, S.; Zhang, X.; Zunger, A. Correcting density functional theory for accurate predictions of compound enthalpies of formation: Fitted elemental-phase reference energies. *Phys. Rev. B: Condens. Matter Mater. Phys.* **2012**, *85*, 115104.
(55) Ganguly, J. *Thermodynamics in Earth and Planetary Sciences*; Springer−Verlag: Berlin, Heidelberg, Germany, 2008.
(56) Darken, L. S.; Gurry, R. W. *Physical Chemistry of Metals*; McGraw−Hill: New York, 1953.
(57) McQuarrie, D. A. *Statistical Mechanics*; Harper and Row: New York, 1976.
(58) Massey, W. S. Cross Products of Vectors in Higher Dimensional Euclidean Spaces. *Am. Math. Mon.* **1983**, *90*, 697−701.
(59) Ambiguously defined facets occur when a set of $d$+1 points (or more) define a ($d$−1)-flat.[47]
(60) Sommerville, D. M. Y. *An Introduction to the Geometry of N Dimensions*; Dover Publications: New York, 1929.
(61) Kresse, G.; Furthmüller, J. Efficient iterative schemes for *ab initio* total-energy calculations using a plane-wave basis set. *Phys. Rev. B: Condens. Matter Mater. Phys.* **1996**, *54*, 11169−11186.
(62) Wisesa, P.; McGill, K. A.; Mueller, T. Efficient generation of generalized Monkhorst-Pack grids through the use of informatics. *Phys. Rev. B: Condens. Matter Mater. Phys.* **2016**, *93*, 155109.
(63) Perdew, J. P.; Burke, K.; Ernzerhof, M. Generalized Gradient Approximation Made Simple. *Phys. Rev. Lett.* **1996**, *77*, 3865−3868.
(64) Blöchl, P. E. Projector augmented-wave method. *Phys. Rev. B: Condens. Matter Mater. Phys.* **1994**, *50*, 17953−17979.
(65) Agapito, L. A.; Curtarolo, S.; Buongiorno Nardelli, M. Reformulation of DFT+*U* as a Pseudohybrid Hubbard Density Functional for Accelerated Materials Discovery. *Phys. Rev. X* **2015**, *5*, 011006.
(66) Taylor, R. H.; Curtarolo, S.; Hart, G. L. W. Guiding the experimental discovery of magnesium alloys. *Phys. Rev. B: Condens. Matter Mater. Phys.* **2011**, *84*, 084101.


DOI: 10.1021/acs.jcim.8b00393
*J. Chem. Inf. Model.* 2018, 58, 2477−2490

(67) Miller, J. Short Report: Reaction Time Analysis with Outlier Exclusion: Bias Varies with Sample Size. *Q. J. Exp. Psychol. A* **1991**, *43*, 907−912.
(68) Leys, C.; Ley, C.; Klein, O.; Bernard, P.; Licata, L. Detecting outliers: Do not use standard deviation around the mean, use absolute deviation around the median. *J. Exp. Soc. Psychol.* **2013**, *49*, 764−766.
(69) Hicks, D.; Toher, C.; De Santo, C.; Levy, O.; Mehl, M. J.; Curtarolo, S. AFLOW-XTAL-MATCH: Automated method for quantifying the structural similarity of materials and identifying unique crystal prototypes. Manuscript in preparation, 2018.
(70) Burzlaff, H.; Malinovsky, Y. A Procedure for the Classification of Non-Organic Crystal Structures. I. Theoretical Background. *Acta Crystallogr., Sect. A: Found. Adv.* **1997**, *53*, 217−224.
(71) Bergerhoff, G.; Hundt, R.; Sievers, R.; Brown, I. D. The inorganic crystal structure data base. *J. Chem. Inf. Model.* **1983**, *23*, 66−69.
(72) Belsky, A.; Hellenbrandt, M.; Karen, V. L.; Luksch, P. New developments in the Inorganic Crystal Structure Database (ICSD): accessibility in support of materials research and design. *Acta Crystallogr., Sect. B: Struct. Sci.* **2002**, *58*, 364−369.
(73) Sato, J.; Omori, T.; Oikawa, K.; Ohnuma, I.; Kainuma, R.; Ishida, K. Cobalt-Base High-Temperature Alloys. *Science* **2006**, *312*, 90−91.
(74) Thorne, L. R. An Innovative Approach to Balancing Chemical-Reaction Equations: A Simplified Matrix-Inversion Technique for Determining The Matrix Null Space. Submitted to arXiv:1110.4321v1, 2011.
(75) Trefethen, L. N.; Bau, D., III. *Numerical Linear Algebra*; Society for Industrial and Applied Mathematics: Philadelphia, PA, 1997.
(76) Kirklin, S.; Saal, J. E.; Hegde, V. I.; Wolverton, C. High-throughput computational search for strengthening precipitates in alloys. *Acta Mater.* **2016**, *102*, 125−135.
(77) Feuersänger, C. *Manual for Package PGFPLOTS*. Available via the Internet at: http://ctan.math.utah.edu/ctan/tex-archive/graphics/pgf/contrib/pgfplots/doc/pgfplots.pdf (accessed Aug. 13, 2018).
(78) Eberz, U.; Seelentag, W.; Schuster, H.-U. Zur Kenntnis farbiger ternärer und quaternärer Zintl-Phasen [Coloured Ternary and Quaternary Zintl-Phases]. *Z. Naturforsch., B: J. Chem. Sci.* **1980**, *35*, 1341−1343.
(79) Hicks, D.; Mehl, M. J.; Gossett, E.; Toher, C.; Levy, O.; Hanson, R. M.; Hart, G. L. W.; Curtarolo, S. The AFLOW Library of Crystallographic Prototypes: Part 2. *Comp. Mat. Sci.* In press arXiv:1806.07864v1, 2018.
(80) Bradley, A. J.; Rodgers, J. W. The Crystal Structure of Heusler Alloys. *Proc. R. Soc. London, Ser. A* **1934**, *144*, 340−359.
(81) Nowotny, H.; Sibert, W. Ternäre Valenzverbindungen in den Systemen Kupfer(Silber)-Arsen(Antimon,Wismut)-Magnesium. *Z. Metallkd.* **1941**, *33*, 391−394.
(82) von Batchelder, F. W.; Raeuchle, R. F. The tetragonal $M\mathrm{Be}_{12}$ structure of silver, palladium, platinum and gold. *Acta Crystallogr.* **1958**, *11*, 122.
(83) The AFLOW Library of Crystallographic Prototypes. *$AuBe_5$ ($C15_b$) Structure*. Available via the Internet at: http://aflow.org/CrystalDatabase/AB5_cF24_216_a_ce.html (accessed Aug. 1, 2018).
(84) Urusov, V. S.; Nadezhina, T. N. Frequency distribution and selection of space groups in inorganic crystal chemistry. *J. Struct. Chem.* **2009**, *50*, 22−37.
(85) Xiang, X.-D.; Sun, X.; Briceño, G.; Lou, Y.; Wang, K.-A.; Chang, H.; Wallace-Freedman, W. G.; Chen, S.-W.; Schultz, P. G. A Combinatorial Approach to Materials Discovery. *Science* **1995**, *268*, 1738−1740.
(86) Takeuchi, I.; Famodu, O. O.; Read, J. C.; Aronova, M. A.; Chang, K.-S.; Craciunescu, C.; Lofland, S. E.; Wuttig, M.; Wellstood, F. C.; Knauss, L.; Orozco, A. Identification of novel compositions of ferromagnetic shape-memory alloys using composition spreads. *Nat. Mater.* **2003**, *2*, 180−184.
(87) Koinuma, H.; Takeuchi, I. Combinatorial solid-state chemistry of inorganic materials. *Nat. Mater.* **2004**, *3*, 429−438.
(88) Curtarolo, S.; Hart, G. L. W.; Buongiorno Nardelli, M.; Mingo, N.; Sanvito, S.; Levy, O. The high-throughput highway to computational materials design. *Nat. Mater.* **2013**, *12*, 191−201.


DOI: 10.1021/acs.jcim.8b00393
*J. Chem. Inf. Model.* 2018, 58, 2477−2490